

Documentation PermaSense

Andreas Hasler

Glaciology, Geomorphodynamics and Geochronology, Department of Geography, University of Zurich, Switzerland.

This documentation gives an overview of the PermaSense data acquisition infrastructure for data users. It comprises the relevant information about the electrical and mechanical setup of the sensors and the WSN hardware (Section 1). Further, technical meta-information and a descriptions of the data processing (Section 2) and the data quality (Section 3), and an overview of the available data and sensor failures (Section 4).

1 Wireless sensor network – hardware setup and technical meta information

The wireless sensor network (WSN) consists of *sensor nodes* and the *base station* (Chapter 3). The different hardware components of the sensor nodes are described in this section. These are different sensors, the logging and communication units (*network node*) and the mechanical protection and installation parts.

1.1 Sensor rods and thermistor chains

The *sensor rods* and *thermistor chains* consist of a mechanical and electrical assembly of 6–14 individual sensing elements (or configurations). In the case of the sensor rod (SR) these sensing elements are four thermistors (YSI–40006) and four electrode pairs (conductive foam) that measure the direct current (DC) resistance of the rock as indicator of its liquid water content (Figure 1). Additionally, the resistance between electrodes at different depths is recorded, but the electrical setup does not support meaningful measurements for the extremely high resistances of this configuration. The sensor rods are placed in near-surface borings with a diameter of 14mm that are drilled perpendicular to the rock surface. A bayonet mounting-tool allows the placement below the surface to avoid direct radiation on the sensor rod. The position of the in-rod electronics at the tip of the sensor rod minimizes measurement errors due to temperature fluctuations (Figure 1). The thermistor chains (TC) measure six to

eight temperatures along a cable that is placed within a rock cleft or in a borehole within steep ice faces. A slight variation of the thermistor chain is the so-called *moisture chain* (TM) that record four temperatures and two resistances of the medium around the cable (simple detection of liquid water).

This three sensor types are electronically very similar and contain the same custom circuit board with two assembly options. Different measurement channels of the sensor elements are switched by the internal electronics of the sensor rod (multiplexer). The measurement signal is transmitted by a DC-voltage to the sensor interface board (SIB) in the network nodes. Beside the real measurements, *reference resistors* within the sensor electronics are recoded as independent references. These resistors are mounted together with *reference resistors of the voltage divider* on the (Figure 2).

Other sensors such as single thermistors or the test setup for self-potential measurements are not presented in this section. The operation of individual thermistors was applied successfully at the Matterhorn field site. Electronically the measurement principle corresponds to the single-ended voltage dividers used within the sensor rods. The self-potential measurements did not provide useful results.

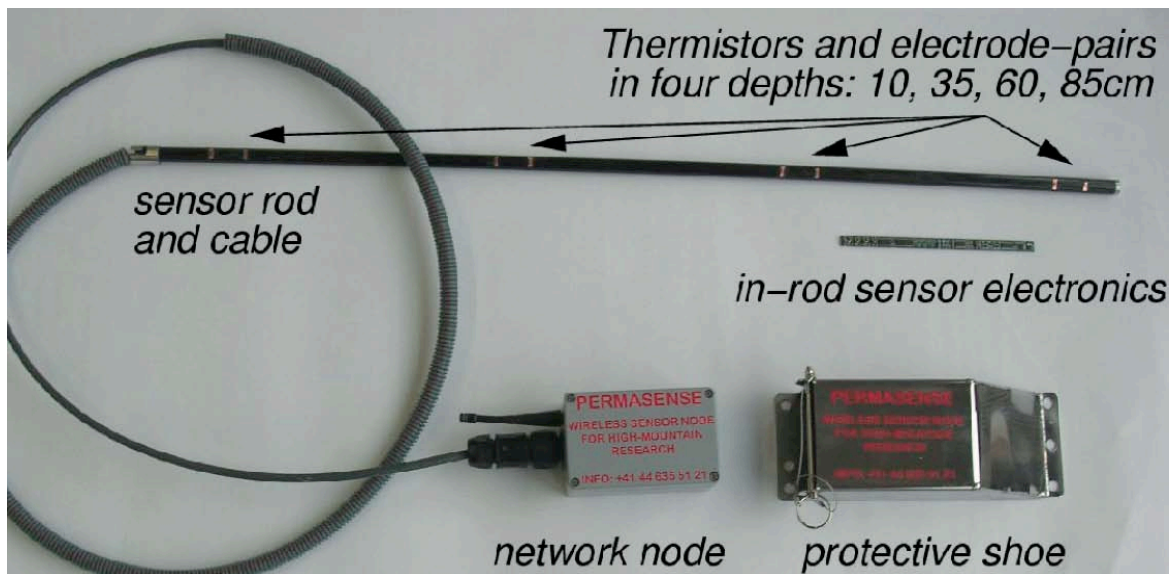


Figure 1: Sensor rod attached to a network node.

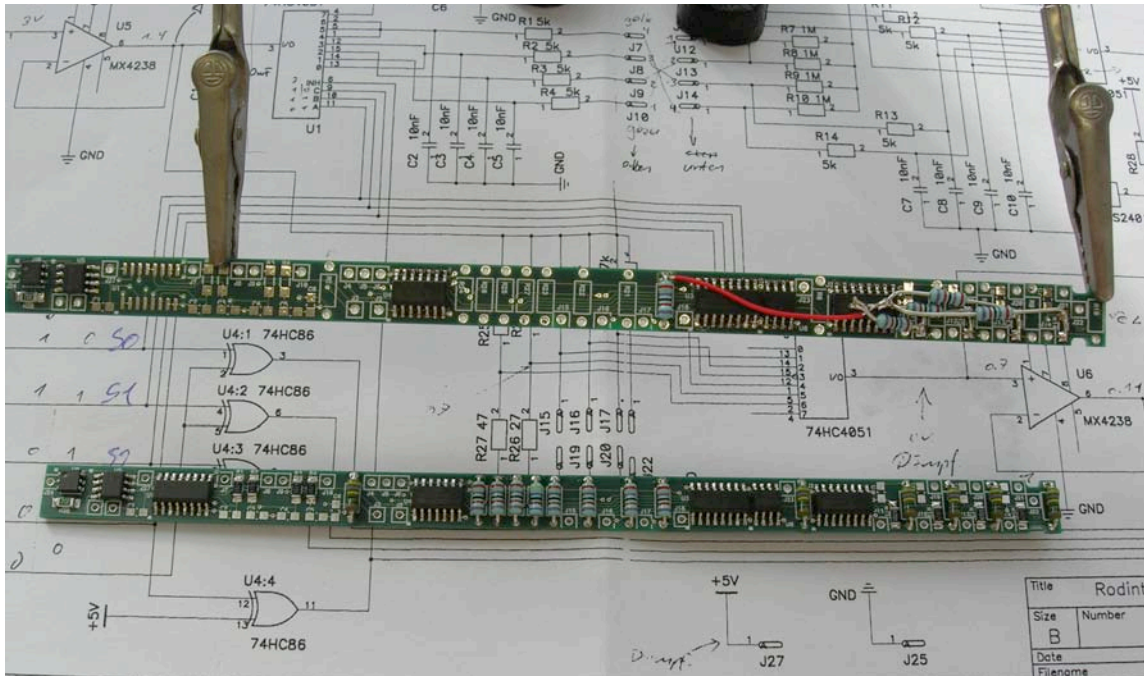


Figure 2: Assembled sensor electronics for sensor rod (bottom) and (termistorchains (top)).

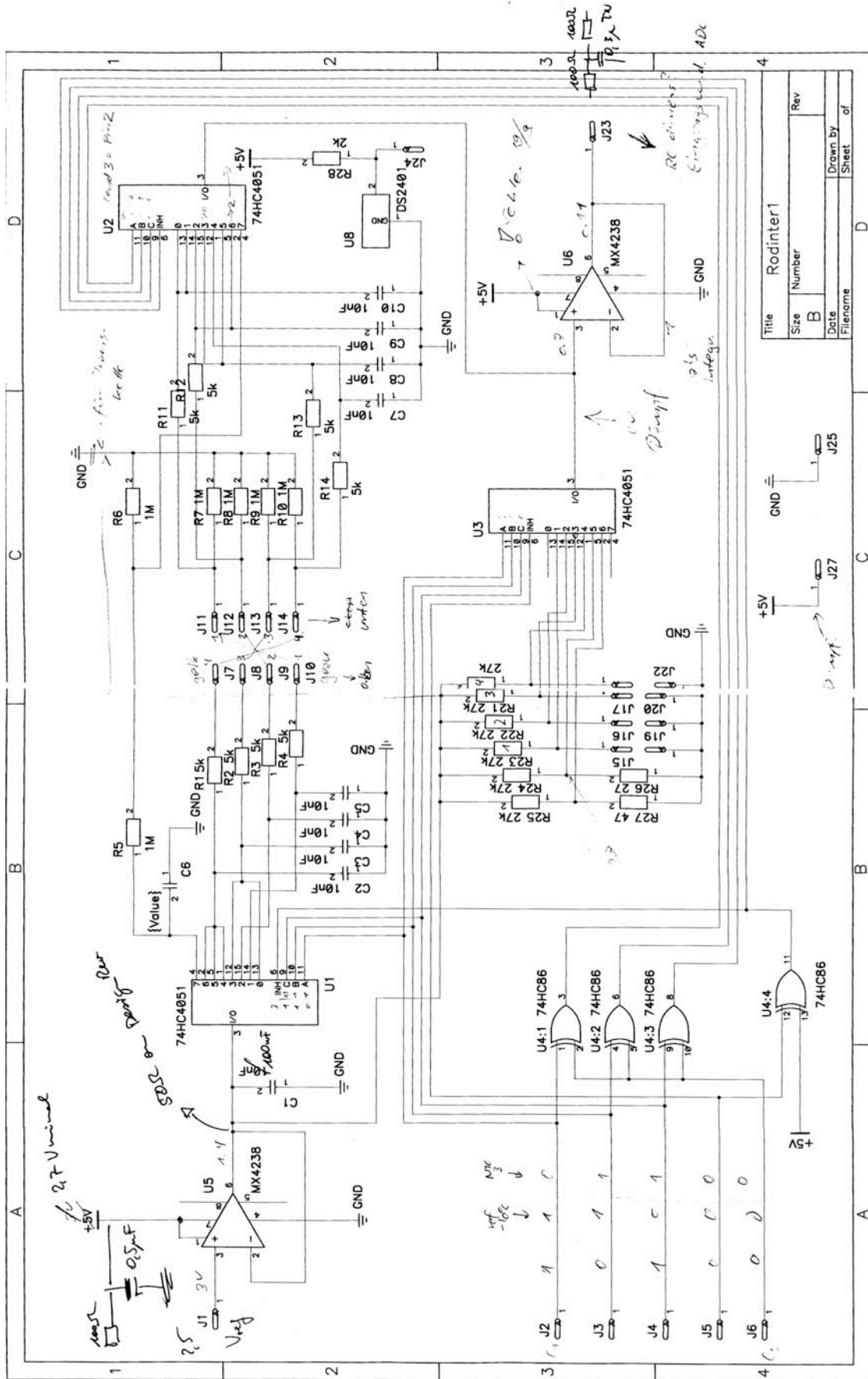


Figure 3: Scheme of sensor electronics

Table 1. Component list of sensor electronics

component	description	provider	ArtNo.	pices	price total
Elektronik board					
MAX 4238 or TS921	OP rail to rail; SO08; replaced for 2. gen OP rail to rail; more stable with cap. load	distrelec	642823	2	7.4
74HC86D	quad EXOR SO14	distrelec	649489	1	0.5
74HC4051D	analog multiplexer 8-cannel SO16	distrelec	649616	3	1.8
74HC7541	oct. Schmitt-Trigger SO20	distrelec	649642	1	3.2
RNM12S	PräzWiderstand 27kOhm 0.1%	distrelec	710431	7	5.25
RNM12S	PräzWiderstand 47kOhm 0.1%	distrelec	710434	1	1
SMA0207	PräzWiderstand 1MOhm 0.1%	distrelec	714662	6	4.8
4816P	Widerstandsnetzwerk SMD 8fach	distrelec	710914	1	2
B37941	Kond.Netzwerk 10nF SMD 4fach	distrelec	823415	3	1.8
	Widerstand 2kOhm SMD	farnell	110-0199	1	0.1
	Seralnr. Chip	farnell	972-5318	1	3
	Print Sensorstab, unbestückt			1	200
	externe Bestückung				
mechanics					
	Glasfaserstab 1m	swiss-comp	125.6095	1	8
	Elektroden			8	40
	NTC Widerstände			4	80
	Alu spitze			1	30
	Messing Endstück mit Bajonettanschluss			1	120
FFA.3E.312	Lemostecker	Lemo	FFA.3E.3 12	1	40
	Kabel 12 pol			1	10
	Litze			1	5
	Füllschaum, Klebstoffe + Dichtmasse	swiss-comp			15
	Kabelschutz				10
costs	für ein Sensorstab inkl. Elektr. und Kabel				588.85

Table 2. Wiring Specification for SIB to 19 Souriau connector:
(Matterhorn set up)

Nr.	PIN saurier connector	PIN SIB 40pin	Name	Description
1	A	1	DGND	digital ground (no ESD protection)
2	B	2	AIN 0	analog input 0; amplified, var. gain
3	C	3	AIN 1	analog input 1; amplified, var. gain
4	D	4	AIN 2	analog input 2; amplified, var. gain
5	E	5	AIN 3	analog input 3; amplified, var. gain
6	F	9	Addr 0	address line 0
7	G	10	Addr 1	address line 1
8	H	11	Addr 2	address line 2
9	J	12	Addr 3	address line 3
10	K	13	Addr 4	address line 4
11	L	14	Addr 5	address line 5
12	M	8 / 24	ADCCOM / AGND	Analog ground
13	N	17	VREF	reference volt. (low resistance)
14	P	18	Sensor ID	sensor identify. line / no cap. ESD!!!
15	R	19	Sensor UART RX (B)	serial port receive
16	S	20	Sensor UART TX (A)	serial Port transmit
17	T	21	SDI_DATA	bidirectional serial line
18	U	22	VCC _{sens}	supply voltage of sensor
19	V	23	VCC _{IN/SDI}	external supply volt. for SIB 4-13V or SDI supply output (9.6 – 16V)

Table 3. Wiring Specification for SIB to 12 Souriau connector:
(Jungfraujoch set up)

Nr.	PIN saurier connector	PIN SIB 40pin	Name	Description
1	G	24	AGND	Analog ground
2	K	2	AIN 0	analog input 0
3	E	9	Addr 0	address line 0
4	D	10	Addr 1	address line 1
5	C	11	Addr 2	address line 2
6	B	12	Addr 3	address line 3
7	A	13	Addr 4	address line 4
8	M	17	VREF	reference volt.
9	J	18	Sensor ID	sensor identify. line / no cap. ESD!!!
10	H	22	VCC _{sens}	supply voltage of sensor

1.2 Applied standard sensors

The geotechnical sensors used at the Matterhorn deployment are:

- a) *ForaPot Crackmeter, ForaNec*: Potentiometric distance sensor that are anchored at the two sides of a cleft and that provide an analogue output signal linearly dependent on the cleft aperture/shear
- b) *Earth pressure cell 3500, Geokon*: Piezometric stress sensor that translate a stress acting on the measurement plane into a DC-voltage proportional to the stress
- c) *Water level transducer 26W, Keller*: Digital stand-alone sensor that calculates the water level from the difference between two piezometric pressure sensors (air, water) and provide digital conversions via RS-485

An overview of these sensors is provided in Figure 18. All the sensors are connected with water-tight connectors (*Souriau*) to the sensor interface board (SIB) in the network nodes. The SIB was designed to provide the stable supply voltage and signal interfaces to these and other standard sensors and allows a flexible combination of different sensors with one network node. All these sensors except the stress sensor where operated successfully, but the pressure sensors did not provide useful information of the hydrological cleft conditions because no water table or ice built-up at the sensor locations. The crackmeters are protected by a shield the reduce the impact of debris fall, snow loading and radiation on the sensors (Figure 4). Further, cables are kept as short as possible to reduce environmental impact.



Figure 4: Overview of applied sensors: Water / air pressure sensor (WP), crackmeter (CR), earth pressure cell (EP), and sensorrod (SR); (other sensors (TC/TM/SP) not shown).

1.3 Network nodes

The hardware of the network nodes comprises the WSN-platform (communication electronics), the sensor interface, power-supply, electro-mechanical parts (antenna, connectors) and the mechanical setup. For the WSN-platform the commercial platform *TinyNode (Shockfish)* was used (see Dubois-Ferrière et al., 2006). The sensor interface and power management (and some additional functions: e.g. system reset; memory extension) are implemented with the SIB. This SIB was developed by an engineering company (*AOT*) based on a user system specification that includes the experience of the first generation network nodes (Talzi et al. 2007) and the extended requirements by the geotechnical sensors (see above). For a technical description of the SIB see Publication II. The power supply is provided by a Lithium-Thionylchlorid non-rechargeable battery (*Saft LSH-20*), which provides stable voltage at very low temperatures for low-power use. Options for external power supply exist. The mechanical setup consists of a rugged aluminum housing (*Bopla*) and a stainless steel protective shoe (Figure 19). This double protection against environmental impact was very successful and no network node experienced serious damage for the whole operation period. The protective shoe has additionally the function to allow a fast node exchange without any tools and reduced the impact of lightnings because the galvanic coupling between housing and protective shoe is low. The shoe was enhanced between the first and the second generation regarding the performance to exchange nodes. The downward orientation of the connector and the antenna (Figure 19) minimizes the impact on these sensitive parts and avoids water entry if the sealing is broken.



Figure 5: Sensor node consisting of the network node inside of the protective shoe (left), a crack-meter below the shield (right) and a thermistor chain inside the cleft (dark cable).

2 Data management and data processing

An overview of the steps of the data acquisition was given in Chapter 3. These are: 1) physical sensing, 2) data logging, 3) data transmission, 4) pre-processing, and 5) archiving. Here we leave out the intermediate parts of the data acquisition (logging and data transmission) because the author made only minor contributions to these parts. Instead the focus is on the pre-processing and archiving with respect to the access to this data by geo-scientists. Processes, which are currently not included in the pre-processing of the PermaDAQ infrastructure are described in a subsequent subsection (Data cleaning, aggregation, and merging). These process may be included in the pre-processing within PermaDAQ in the future. At the end of this section the applied analysis tools for off-line processing are outlined.

2.1 Data structure, pre-processing, and data access

The data arrives divided into different data packets at the data backend server: For each point in time of the logging 2–5 data packets are generated and transmitted to the server which runs a software for data streaming (GSN: see Publication II). The types of data packets are *MUX1* and *MUX2* for the multiplexer data (sensor rods, thermistor chains, and moisture chains), *ANL* for the other analogue measurements (crackmeters, individual thermistors, and earth pressure cells), and *DIG* for the digital water table sensors. A fifth sensor data packet type (*DIFF*) for the self-potential measurements exists but is not described for the further processing. The same is true for the health data that monitors parameters of the network nodes.

In a first step, these system specific processes are performed and the data is dumped into a SQL database. In a second step this raw data is converted into physical units (°C, mm, MPa, ...) based on meta-information of the attached sensors and assigned to the measurement locations. This converted data is stored in a second database that is accessible for the users with separate tables for each data packet type. This data base contains many tables that most are not used for the data access. The relevant tables start with *matterhorn* or *jungfraujoch* and have a suffix for the sensor type. E.g. the table *matterhorn_sensorrod1* contains all data from *MUX1* of the sensor rods at Matterhorn. For details see the extended version of this documentation (*sensor_docu.pdf*). For the crackmeter data there are 5 sub-types with separate tables. Each table is for a certain combination of sensors attached to the 4 channels of the analog-digital converter (ADC) (Table 2). There are 4 letters representing the sensors attached to the 4 channels of the ADC. E.g. *nctn* means that channel 0 and 3 has no sensors connected, on channel 1 is a crackmeter, and on channel 2 there is a thermistor. Table 4 provides the primary meta data that is needed for the access of this data. The data is accessed by MySQL commands. Automated routines for this data access are implemented for the R data analysis software and are described in the next subsection and the extended documentation. Alternatively tools to export csv-files are provided by the data front-end on <http://data.permasense.ch/>.

Table 4. Primary meta-information for data access:

pos	MUX	ANL	DIG
jj01	SR		
jj02	SR		
jj03	SR		
jj04	SR		
jj05	SR		
jj06	SR		
jj07	SR		
jj08	TC		
jj09	SR		
jj10	TC		
mh01	TC	nctt	
mh02	TC	nctt	
mh03	TC	nctt	
mh04	TC	nctt	
mh05	TM	EP	WP
mh06		tctc	
mh07	TM	EP	WP
mh08		nctc	
mh09		ccct	
mh10	SR	ntnn	
mh11	SR	ntnn	
mh12	SR	ntnn	
mh13		SP	
mh20		ccnn	
mh21		ccnn	
mh22		ccnn	

Table 5. Fields and first values of table: "matterhorn_thermistorchain":

```

=====timestamp and system=====
"PK"
"timed"
"POSITION"           position of measurement
"DEVICE_ID"          node ID that made measurement
"GENERATION_TIME"    time stamp of measurement in ms since 1.1.1970
"TIMESTAMP"
"SENSORTYPE"         e.g. "SR"
"SENSORTYPE_SERIALID"
"HEADER_SEQNR"
"HEADER_ORIGINATORID"
"HEADER_ETIME"       time span from measurement until arrival in base station
"PAYLOAD_SAMPLE_VALID"
"PAYLOAD_SAMPLE_NO"  nb. of sample (measurement) 2 byte repeating, not unique!
=====measurements=====
"TC_REF1"            reference measurement (2°C)
"TC_REF2"            reference measurement (-9.8°C)
"TC_T1"              top temperature (0m; for matterhorn!)
"TC_T2"              temperature (0.5m)
"TC_T3"              temperature (1m)
"TC_T4"              temperature (1.5m)
"TC_REF3"            reference measurement (2°C) 2nd
"TC_REF4"            reference measurement (-9.8°C) 2nd
"TC_T5"              temperature (2m)
"TC_T6"              temperature (2.5m)
"TC_T7"              temperature (3m)
"TC_T8"              temperature (3.5m)
=====

```

2.2 Data merging, filtering, and aggregation

For an efficient analysis the data should be ordered by sensor node because the ease direct extraction of time series and cross-correlations. The data may be identified by the sensor node and the sensing element label (e.g. *mh01 – TC_T3* stands for thermistor 3 of sensor node 1 at Matterhorn). To get the data in that order, the data from the same sensor node in the different tables (see above) needs to be merged. Because the different data packets (MUX1, MUX2, ...) have slightly different timestamps for the measurements of the same logging cycle, a simple merging by time is not possible. Two possibilities to do this merging are implemented for different data types: a) for the MUX data the sample number and the timestamp is used for merging; b) the data is first aggregated to regular timestamps and merged subsequently. The more intensive version a) is required by the filtering algorithm for the MUX data. This filtering applies the values of the *reference resistors*, which are measured together with the real measurements (see Hardware setup): If the reference values is not within a defined range (see sensor_docu.pdf) the data is considered as invalid and not used for the analysis. For all non-MUX sensors a visual control and a masking of the invalid data is applied (see Table 2).

The temporal resolution of the raw data is currently 2 min allowing down sampling and aggregation of the data. The current implementation with MySQL by the query generation routines makes an average over the interval $[t-(intv/2) : t+(intv/2)]$ (with t = timestamp and $intv$ = aggregation interval in minutes) and assigns the values to the timestamp. The level of aggregation (or measurement interval) depends on the characteristics of the data and the purpose the data use (Hall, 1997). With increasing size of the averaging interval the amplitude of the time series is less represented in the dataset and the values deviate more from the effective temperature measured at this point in time (Figure 6). For the rock surface temperature (2cm) with strong radiation influence and large daily amplitudes, such as at position mh10 (Figure 6), precise representation of the raw values and short term fluctuations is given on a aggregation with a granularity of 10 minutes or smaller, while the daily evolution and amplitude is still well represented on a 30 minutes level. Larger averaging windows are not suitable to represent surface temperature variations on rock and underestimate temperature peaks. For temperatures at greater depth larger aggregation intervals may be suitable and allow data reduction if non-conductive effects can be neglected.

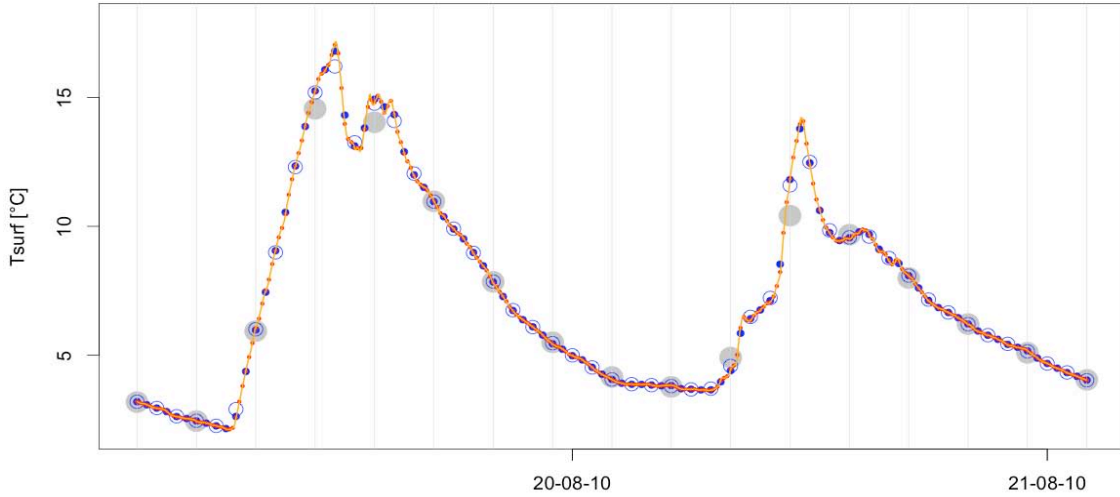


Figure 6: Effect of aggregation levels on the example of T_{surf} of mh10: raw data (orange line), 10 min av. (red), 30 min av. (blue), 1 hour av. (blue circle) and 3 hours av. (grey). Co-centric circles indicate good representation of the instantaneous value.

The difference (ΔT) between down sampling by averaging or by linear interpolating for 10 min intervals at mh10 has a standard deviation $stdev(\Delta T1)$ is 0.032 °C, $stdev(\Delta T2)$ is 0.013 °C and $stdev(\Delta T3)$ is 0.005 °C. Hence, with a ten minutes interval the aggregated data is valid for both, representation of the instantaneous value and mean of the 10 minutes time period.

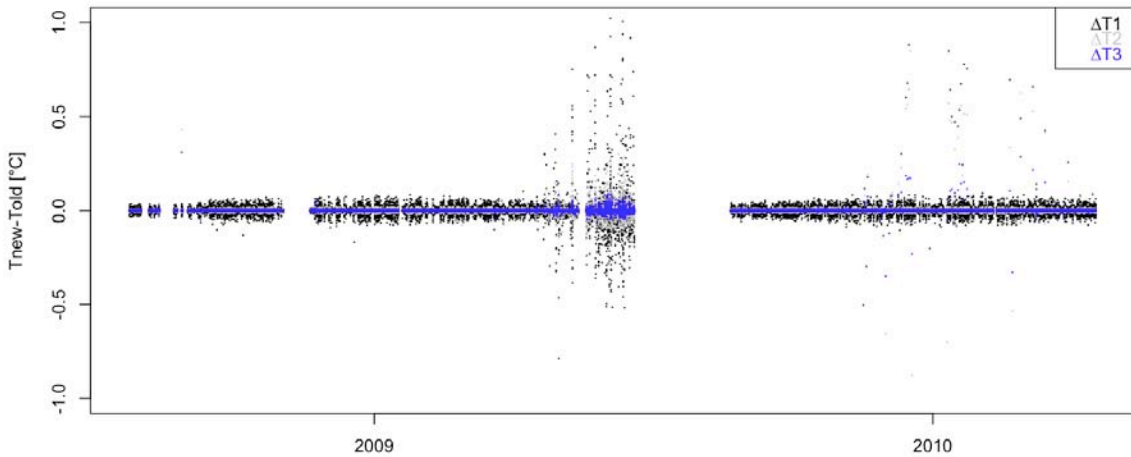


Figure 7: Difference between averaging (new) and interpolating (old) procedure for data aggregation on 10 min intervals at mh10 and verification of data processing (independent procedure). The standard deviation $stdev(\Delta T1)$ is 0.032 °C, $stdev(\Delta T2)$ is 0.013 °C and $stdev(\Delta T3)$ is 0.005 °C.

2.3 Analysis tools

The analysis tools used for this thesis comprises diverse plotting routines for time series, cross-correlations, 2-dimensional movement patterns and spectral analyses that are implemented in R (sensor_docu.pdf) and comparison between modeled and measured temperatures assuming conductive heat flux (*DeltaCon*) that is written in the interactive development language IDL. Further, functions to fill data gaps for mean annual temperature calculation (MAT) were applied (Publication III). The procedure of the time series and cross-correlation plots are described in Publication III and V.

A spectral analysis was applied in earlier studies for the detection of non-conductive heat fluxes (Hinkel and Outcalt, 1993). Examples for such an application is given in Appendix A.6. There a short time fourier transformation (STFT) is used to calculate the power spectrum of the frequencies within 2-day windows that are shifted with 12 hours increments. The tool *DeltaCon* calculates the temperatures of the two intermediate thermistors of the sensor rods (SR_T2, SR_T3) for a point in time based on the measured temperatures of the previous time step and the uppermost and lower most temperature. The temperature difference of the modeled and measured temperatures at SR_T2, SR_T3 is converted into a source term of the non-conductive heat flux (Gerber, 2010). Both methods, the spectral analysis and *DeltaCon*, produce comparable results, but *DeltaCon* is restricted to temperature profiles with clearly defined depths of the thermistors (Appendix A.6). Contrary, *DeltaCon* gives a rough indication how large the non-conductive heat fluxes are.

3 Data quality

During the testing phase and two years of operation of the PermaSense WSNs, diverse evaluations of the data quality have been undertaken. Some of these results are contained in Beutel et al. (2009), Hasler et al. (2008) or internal reports (Hasler and S. Gruber, 2009). A complete quantitative data evaluation can not be presented within this study because of the lack of automated data checking algorithms (visual control is still one of the most reliable methods) that would be necessary to treat this amount of data. Here different aspects of the data quality and characteristics are illustrated in an exemplary manner. The basic terms used hereto are:

- *Absolute accuracy* in the sense of how correct the measurement quantity at the sensing element is represented in the dataset (measurement error).
- *Stability* or *relative accuracy* means how much the measurement value is independent of effects other than the measurement quantity within a time series. (In contrast to other definitions, here relative accuracy is not used for the accuracy between different sensing elements, because this corresponds quite much to the absolute accuracy in this case (measurement errors are little dependent).
- *Representativity* of a measurement says how good a measured value at the sensing element represents the physical quantity to be measured in the undisturbed situation (physical effect of the instrumentation). This effect may also be considered in the term absolute accuracy (or better *total accuracy*) in many studies, but it is rarely addressed explicitly.
- *Precision* means the number of digits with which the data is measured, stored, transmitted or represented. Note that measurement precision (ADC-resolution) may differ from transmission/representation precision.

The reliability of the system is evaluated by the completeness of the data and by the time delay with which the data was delivered to the data backend, the first being essential for an environmental science instrument and both being important for environmental monitoring and early warning.

3.1 Temperature measurements:

The following quality analysis is the basis for the application of the temperature data in Publication III and V. A summary of this analysis is contained in the respective publications.

The internal references of the sensorrods and the thermistorchains (see section 1) are used as an indicator of proper functionality of the measurement and for the quantification of the measurement accuracy and stability. The stability of these references has two different characteristics that are valid for the measurements as well: First, fluctuations within a consistent measurement series caused by temperature fluctuations and electrical “noise”. Second, an offset between series with exchanged hardware (different WSN-nodes in different *deployments*).

Figure 8 shows two examples of this reference stability, one from a thermistorchain and the other one from a sensor rod. The fluctuations due to temperature variations (mh03) lie within 20 mK and the offset due to different nodes attached (before and after June 23th) is below 5 mK. Both values are clearly smaller than the range of the thermistor accuracy defined by the supplier ($\pm 0.2^{\circ}\text{C}$; no successful calibration was made). Some single measurements of the thermistorchain show higher deviations that may be caused electronically. If they exceed a tolerance of $2\pm 0.15^{\circ}\text{C}$ the sample is filtered (section 2). The raw data is transmitted with a two-byte precision resulting in a 1.3 mK resolution (horizontal stripes in Figure 8). The resulting absolute accuracy of the measurement system itself is $\pm 0.3^{\circ}\text{C}$. Relative accuracy within a time series is clearly better in case of non-occurrence of electronic instabilities.

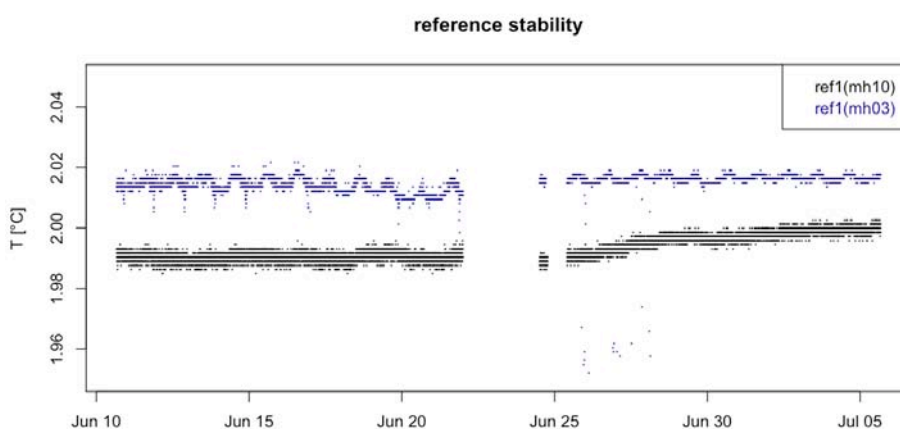


Figure 8: Stability of reference values during node exchange at June 23th 2010 of thermistorchain mh03 (blue) and sensorrod mh10 (black).

The representativity of a temperature measurement depends strongly on the physical sensor design and the thermal parameters of the measurement media. The high heat capacity of rock and the proximity ($< 1\text{mm}$) of the thermistor to this *thermal mass* increases the representativity of the measurement. The effect of direct thermal coupling through the thermistor wires can be neglected with the given sensor design (wires are lead from inside towards the surface; smaller gradients), but heat may be transmitted from the bypassing wires to the thermistor. This influence may be relevant only for the upper most sensor of the sensorrod. Numerical modeling of this setup would help to quantify this source of error. So done for the laboratory experiments (with slightly different setup), the error was smaller than 0.01°C for a 10°C cable temperature disturbance at 10cm distance. For the measurements of the cleft temperatures, the representativity is much lower. First, the thermistor chain measures a mix between cleft air temperature and cleft surface temperature, and second, disturbances through the wires will affect the measurements much more due to bad thermal connection with the measurement media (in case of ice infill significantly better). Thus, the cleft temperature must be interpreted with an uncertainty in the range of $\pm 2^{\circ}\text{C}$.

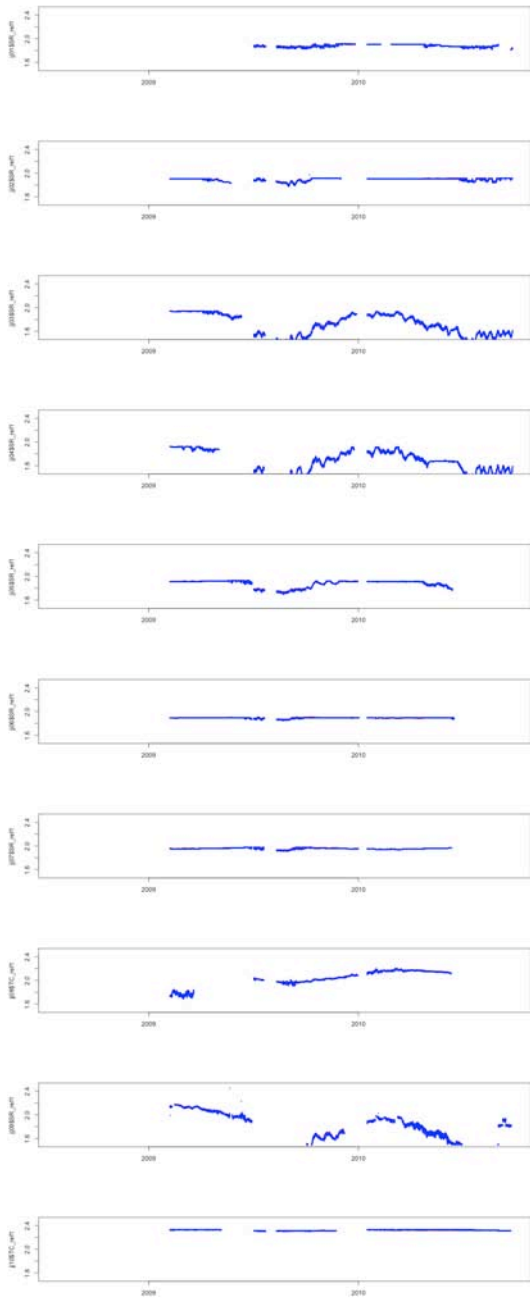


Figure 9: Reference stability of sensors at Jungfrauoch.

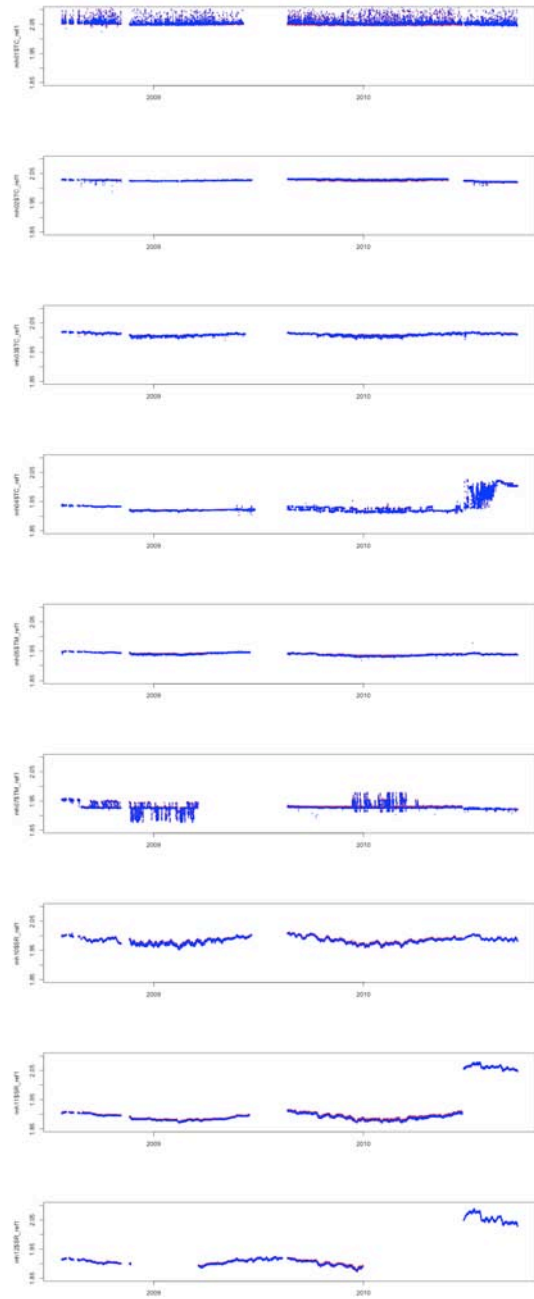


Figure 10: Reference stability of all MUX-sensors at Matterhorn. Comment: mh11 and mh12 show a significant change in the reference values at the node exchange in June 2010; mh04 has a change in the reference values when the crackmeter connector was repaired (change of el. load); mh01 and mh07 have electrical instabilities that are filtered based on this ref. values.

3.2 Rock resistance:

In terms of accuracy and precision the rock resistances measured by the sensorrods have similar characteristics as the temperature measurements as they are electronically identical. This means that the absolute accuracy is $\pm 1 \text{ k}\Omega$ if the measured value is $1 \text{ M}\Omega$ but the accuracy decreases dramatically for large resistance values ($\pm 200 \text{ M}\Omega$ at $1 \text{ G}\Omega$; upper limit of range). The representativity of the resistance measurements depends on the contact resistance of the electrodes and on local heterogeneities of the rock between these electrodes. In contrast to ERT-surveys the contact resistance is directly added to the rock resistance (serial connection). Pre-tests with the applied conductive foams showed, that contact resistances are below $5 \text{ k}\Omega$ if installed on a clean rock surface. Because of the in-hole installation of the electrodes, the cleanness of the contact can hardly be controlled. Temperature-resistivity gradients for intact porous rock in frozen state lies in the range of $20\text{--}40 \text{ \%/}^\circ\text{C}$ cooling (Krautblatter, 2009). Larger temperature dependency in the measured data (Appendix A.8), indicate that the measurements on the north side of Jungfrauoch (jj05–jj09) are influenced by variations of the contact resistance or micro clefts between the electrode pair.

3.3 Cleft movements:

The potentiometric dilatation measurements have little electronic sources of errors as they do not contain any electronics and thermal changes of the total potentiometer resistance are compensated by the bridge circuit measurement design. Hence, the electronical accuracy depends only on effects on the sensor interface board (SIB) that are in the order of the measurement precision ($\text{CR-range}/65000 = 15 \text{ ppm} = 0.8 - 5 \text{ }\mu\text{m}$). Effects due to thermal expansion of the materials are compensated mechanically within the instrument.

Errors due to rapid change in irradiation (leading not equilibrated instrument temperatures) are analyzed by changing the crackmeter mh01 from being mounted across the cleft to a setting with both displacement anchors at the same side of the cleft (on an intact rock mass). Figure 11 shows this change from across-cleft to intact-rock dilatation, illustrating the good thermal stability of the crackmeter measurements even with enormous temporal temperature gradients ($\approx 10 \text{ }^\circ\text{C/h}$ at 2 cm from rock surface). While the linear expansion of the cleft was $-6 \text{ }\mu\text{m}/^\circ\text{C}$, the on over the approximately 150mm intact rock between the anchors is $+0.1$ to $+0.2 \text{ }\mu\text{m}/^\circ\text{C}$ for daily temperature fluctuations. This dilatation signal may be explained by thermal expansion of the rock, hence no significant measurement error is detected (Hasler 2011). This is clearly better than the supplier's specification $5 \text{ ppm}/^\circ\text{C}$ (being $0.25 \text{ }\mu\text{m}/^\circ\text{C}$ for 50 mm CR-range) even for this very fast temperature fluctuations.

No node change at position mh01 was performed since the modification of the crackmeter position, therefore its effect could not be quantified with this stable time series. Never-the-less time series from other sensors (see: Supplementary material) indicate no significant offsets in the crackmeter data when node changes were performed. In analogy with the sensorrod data, this offset is assumed to be in the order of the measurement precision (15 ppm). Hence, the crackmeter accuracy is ± 3 to $\pm 18 \mu\text{m}$ (± 50 ppm of the measurement range, 50 to 300 mm CR-range).

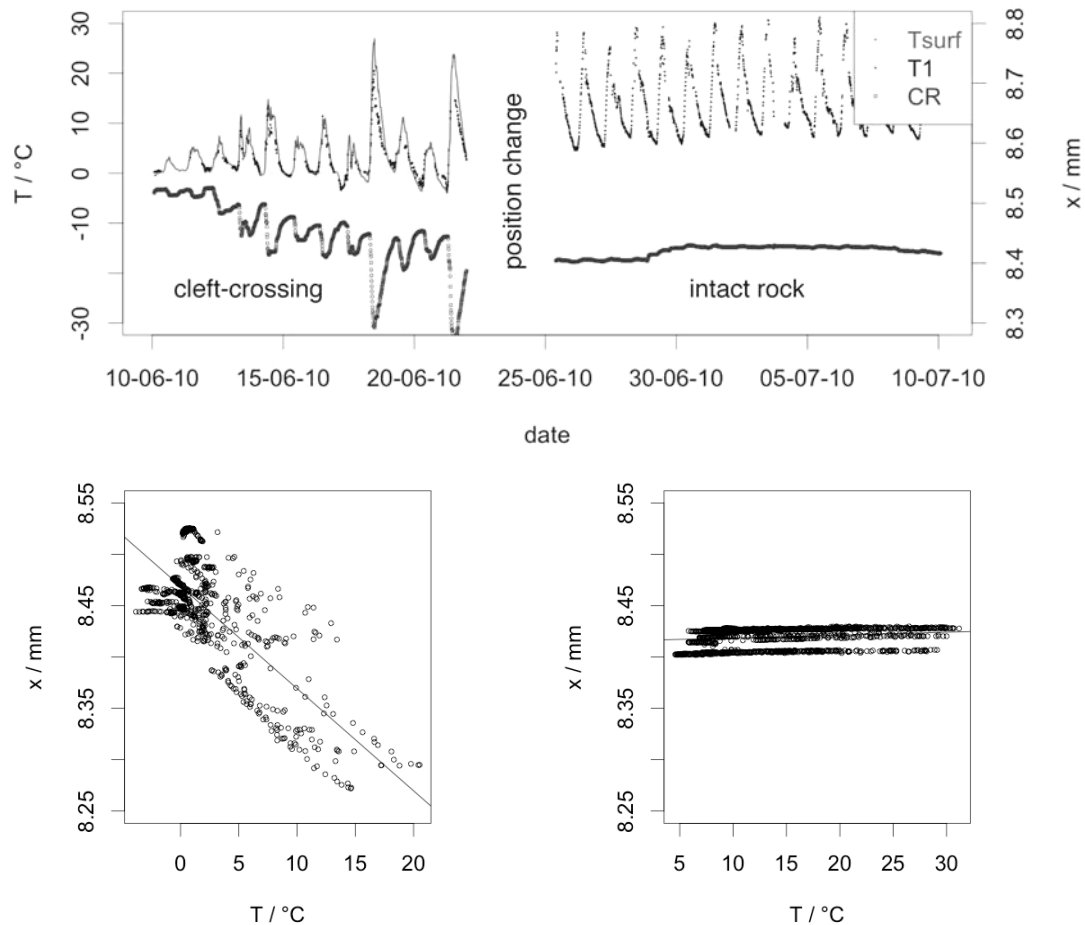


Figure 11: Stability of crackmeter measurements: Time series of dilatation and cleft temperatures and instrument Temperature before (top – June–July 2010) change from cleft to plain rock (Figure 5 in Publication V); dilatation (ΔCR) as a function of the surface temperature (T_{surf}) in June 2010 (bottom left) and July 2010 (bottom right).

3.4 Water pressure and stress sensors

The hydrological and stress sensors placed in two clefts were not frozen in or flooded during the two years of measurements available. This corresponds with observations made in several site visits. Because this series are not used for the analysis in this study, an evaluation of the data quality is passed. Just the functionality of these sensors is briefly summarized: The digital hydrological sensor measuring air and water pressure (and the

temperature of both sensing elements) did register reliable values for the whole time the system was operating (Figure 12). The pressure within the cleft (water sensor) and at the rock surface (air pressure) follow each other closely, hence, no water column is detected.

In contrast, the earth pressure cell did not register reasonable values. This is on one hand due to the missing ice aggradation around the sensor, but the analysis of the values indicates an additional technical problem: An error in the logging routine writes the channels 0–2 instead of channel 1–3 of the ADC to the respective data fields. Hence, the instrument temperature (measured as controlling parameter) of the earth pressure cell is written into the field for the stress data (EP_P) with the conversion for the latter parameter. However the instrument temperature and earlier tests in the laboratory indicate that this problem could be corrected easily and that future operation of this sensor type will be successful.

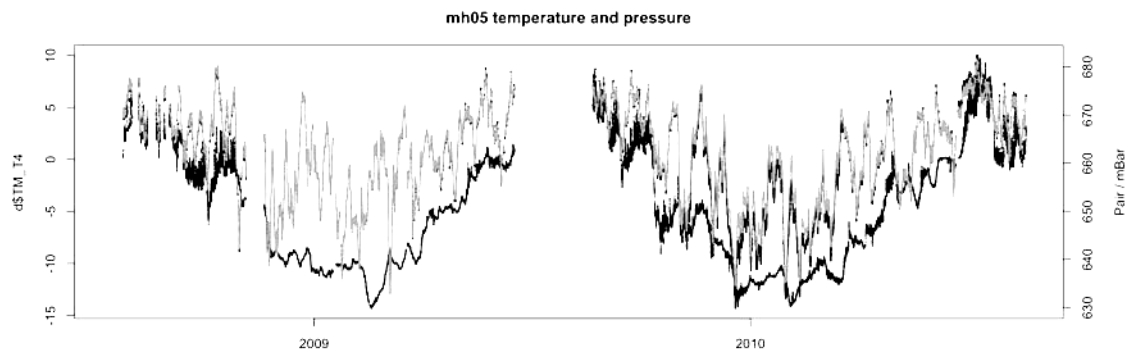


Figure 12: Hydrological measurements at mh05: temperature of the moisture chain T4 (black), air pressure (dark grey) and cleft water pressure in 3 m depth (light grey). The air and water pressure are closely correlated.

4 Data integrity

For geo-science it is often important to have continuous time series over long (multi annual) time spans. Three types of missing data may be distinguished in our system: a) A sensor node fails regarding data logging or transmission and all measurements for the given time span is missing. b) The sensor rod (or thermistor chain) fails and invalid data is transmitted. c) One individual sensing element fails due to physical damage. This section gives an overview of the available data and illustrates the evolution of the system performance of the WSN in terms of data delivery. Further a list of the failed sensing elements (e.g. thermistors) is provided.

4.1 Overview of data integrity

In Figure 13 the data integrity of each sensor node is illustrated with respect to the type a) and b) data gaps. The failure of individual sensing elements is not considered in Figure 13. Hence, the grey area shows how much of the data acquisition is correct in terms of measurements, logging and transmission. The black lines show how fast the data is available (assuming proper transmission from the base station to the server and correct server operation; this is usually the case).

Four sensor nodes (mh09, mh20, mh21, and mh22) were installed in summer 2010 and have no data prior to this date (Figure 13). The low values at mh01 are explained by a malfunction of the sensor rod and consecutive filtering. Due to the high sampling rate interpolation of the missing values is still possible. Sensor node jj01 shows a data gap since October 2010 due to snow cover on the network node (Figure 13). This data will be automatically delivered in spring when connection is re-established. In summer 2010 this “flushing” function worked properly after a base station failure (transmission delay of all jj nodes). The sensor rod at jj09 has most likely an error in the addressing of the multiplexer of the sensor rode (wrong pin connection) and much of the data is filtered due to this (Figure 13). Since summer 2010 only two gaps of each about one month exist (mh08, mh09). These two network nodes run out of power and were replaced. This low power situation was detected in advance by system monitoring tools (<http://data.permasense.ch/>) but weather conditions and availability of personnel are the reasons for these gaps. Regarding the transmission delay the data is available with only 30–120 seconds delay since summer 2010. The current status of data integrity and system behavior is very satisfying.

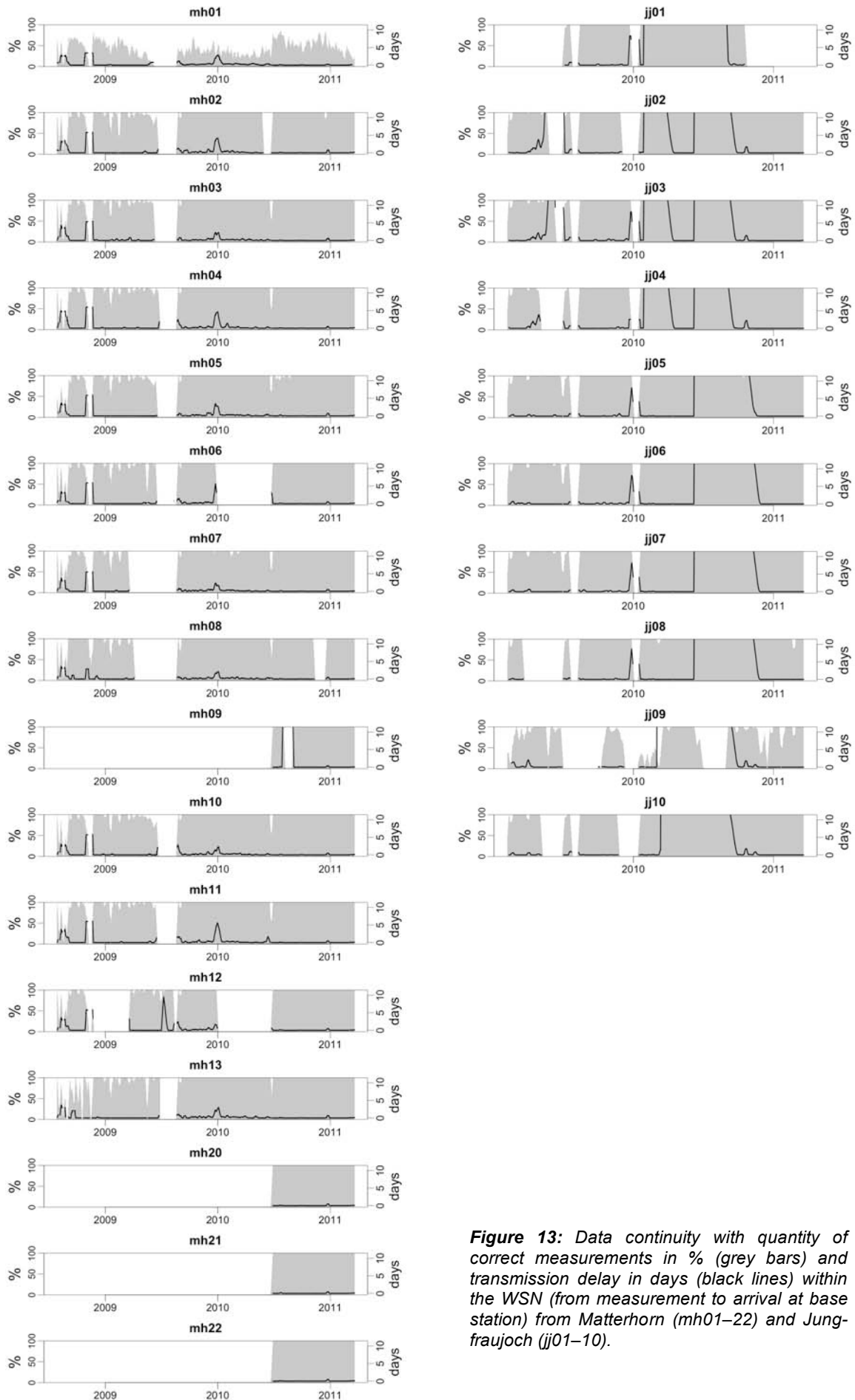


Figure 13: Data continuity with quantity of correct measurements in % (grey bars) and transmission delay in days (black lines) within the WSN (from measurement to arrival at base station) from Matterhorn (mh01–22) and Jungfrauoch (jj01–10).

4.2 Overview of sensor failures and data gaps

Table 6 summarizes the gaps in the data from Jungfraujoch and Matterhorn. All the three mentioned types (a, b, c) of missing data is considered. The information about broken thermistors of Table 6 is used to filter this invalid data because no automatic detection is possible in these cases.

Table 6. Notes of data gaps and broken thermistors:

Matterhorn:	Jungfraujoch:
all mh nodes: gaps from mid June 2009 to mid August 2009 (except mh12) and in Nov. 2008 mh01 instability of sensor rod for whole period	all jj nodes: gaps in Aug 2009 and Jan 2010 Hardware error at jj09 (wrong addressing, pin connection mistaken)
mh01: gap in Tsurf after exchange June 2010 mh02: gap in Tsurf after exchange June 2010 mh03: gap in Tsurf after exchange June 2010 mh04: no Tsurf after exchange June 2010, broken thermistor mh04: no CR before June 2010 mh06: gap in CR from Jan to June 2010 mh07: long gap before June 2010 mh08: gap in CR from April to August 2009, gap in CR after exchange June 2010, gap in October 2010 mh09: gap in July and August 2010 mh12: gap in MUX Nov. 2008 to March 2009 and Jan. to June 2010	large gaps at jj01, jj08 and jj10
broken thermistors: mh02: T3, T4, T7, T8 mh12: T3	broken thermistors: jj02: T2, T3 jj03: T2 (occasionally) jj04: T1, T2 jj07: T2